TERRASAR-X DATA FOR IMPROVING GEOMETRIC ACCURACY OF OPTICAL HIGH AND VERY HIGH RESOLUTION SATELLITE DATA

P. Reinartz*, R. Müller, S. Suri, P. Schwind, M. Schneider

German Aerospace Center (DLR), Remote Sensing Technology Institute, 82234 Wessling, Germany - (peter.reinartz, rupert.mueller, sahil.suri, peter.schwind, mathias.schneider)@dlr.de

Commission I, WG I/2

KEY WORDS: Orthorectification, Automatic Ground Control, Orientation Improvement, TerraSAR-X, Optical/SAR Integration,

ABSTRACT:

Most high resolution optical images from space need ground control information (GCP) before an orthorectification can be performed. The very high geometric accuracy of geocoded data of the TerraSAR-X satellite has been shown in several investigations. This precision has been reached fully automatically without any GCP and is due to good sensor calibration, high accuracy of satellite position and the low dependency on the satellites attitude solution. Therefore TerraSAR-X data can be used as "ground control" to improve the exterior orientation and thereby the geometric accuracy of orthorectified optical satellite data. The technique used is the measurement of identical points in the images, either by manual measurements or through local image matching using adapted mutual information (MI) and to estimate improvements for the exterior orientation or Rational Polynomial Coefficients (RPCs). To be able to use this intensity based method, the radar data have to be filtered before starting the matching procedure. Through adjustment calculations falsely matched points are eliminated and an optimal improvement for the attitude angles is found. The optical data are orthorectified using these improvements and the available DEM. The results are very promising and compared using conventional ground control information from maps or GPS measurements.

1. INTRODUCTION

Orthorectification of high (HR) and very high resolution (VHR) optical satellite data using direct sensor orientation still needs ground control information to reach absolute geometric accuracy in pixel or sub-pixel range (Reinartz et al. 2006). This is mainly due to the insufficient knowledge of the satellite attitude and thermally influenced mounting angles, which lead to location errors between 5 m and several hundred meters depending on the sensor/satellite. Ground control information can be obtained by several means: such as measuring GPS points in situ, measuring points in topographic maps or using reference images already orthorectified together with height information from a suitable Digital Elevation Model (DEM) (Jacobsen, 2006). In the case of reference images matching procedures can be applied to extract tie points automatically and to improve the exterior orientation parameters (Müller et al. 2007). The drawback is that up to now optical reference images are in most cases not easily available. Especially for very high resolution data with pixel sizes of 2.5 m and lower, only few areas around the world are covered by orthoimages which reach this high geometric precision to serve as a reference.

The German Aerospace Center (DLR) operates the TerraSAR-X satellite since June 2007. A detailed analysis by several independent institutions such as the National Geospatial-Intelligence Agency (NGA), has shown that the geometric accuracy of the orbit errors are as small as 20 centimeters and the range errors are well under 1 meter (Ager et al. 2009; Schubert et al. 2008). Atmospheric properties which influence the runtime of the signal have to be taken into account to reach this very high performance. The EEC product shows absolute geolocation accuracies in the meter range for rural areas. These high accuracies can only be reached if the digital elevation model, which is needed for the processing exhibits also accuracies in this range.

Since mainly distances are measured, the geometry of radar data from space borne sensors is not much dependent on the attitude of the satellite due to the spherical waves which are emitted from the microwave antenna. Since the accuracy of TerraSAR-X is better than 1 m in the Single Look Slant Range Complex (SSC) mode, the same spatial accuracy can be reached in the Enhanced Ellipsoid Corrected (EEC) mode if the data are rectified using a high precision DEM. In order to combine the high geometric potential of TerraSAR-X with the necessary improvements of the exterior orientation parameters of HR and VHR optical sensors several investigations are shown in this paper. Since radar and optical data show a very different behavior, a simple correlation technique is not applicable. Tie points can therefore be found either by manual point measurements or by automatic multimodal image registration techniques like Mutual Information (Suri et al. 2008). We show the usage of both methods and their combination for the purpose of using TerraSAR-X data as geocoding reference for the orthorectification of optical data from e.g. IKONOS data. The resulting orthorectified images are compared with check points from other sources for their geometric properties. Due to the different nature of the images, the tie points are mainly taken from relatively flat rural areas including streets. Urban areas and forested areas are generally not well suited for the process due to the different object geometries in radar and optical data respectively but also the behavior of the matching process for these land cover classes are investigated. Some filtering processes for the radar data for these areas improve the possibility to match optical and radar data by mutual information algorithms significantly. The results shown are very promising especially for the automatic technique but some difficulties arise depending on radar backscatter properties.

2. TIE POINTS FROM RADAR DATA

In order to use the TerraSAR-X data as ground control source (GCPs) for the improvement of the measured attitude data of the optical data, homologous points (tie points) in the two images have to be found. This can be done either by manual/visual measurements, or by automatic techniques using multimodal image matching. Since the image information of both data sets is very different due to geometric and radiometric acquisition properties, this is not a straightforward procedure.

2.1 Visual Interpretation

When looking at a TerraSAR-X scene, the human interpret can visually classify some objects/features almost as well as in optical images. Thus, one of our first thoughts was to try a manual/visual measurement of tie points and use them as GCPs. However, the different characteristics of optical and radar imagery have to be considered. Especially the typical radar effects like foreshortening, shadowing etc should be accounted for when selecting GCPs manually. Selected GCPs should be situated in flat terrain and they should not be surrounded by trees or high buildings. During the tests, street crossings in agricultural areas as well as the center of roundabouts turned out to be good GCPs. However, the visual measurement is still very challenging and needs an experienced operator.

2.2 Mutual Information

To find conjugate features within SAR and optical images automatically, intensity based registration metrics like Mutual Information (MI) have been considered in the past for image of resolution in 5-10m. MI has evolved from the field of information theory (Viola, 2009), (Collignon et al. 1995) and it describes a statistical dependence between two random variables (e.g. A and B) expressed in terms of variable entropies. In case Shannon entropy (additive in nature) is selected to represent the individual variable information, mutual information between two variable A and B is defined as:

$$MI(A,B) = H(A) + H(B) - H(A,B) \tag{1}$$

where H(A) and H(B) are the Shannon entropies of A and B respectively, H(A,B) is the joint variable entropy. Considering A and B as two remote sensing images their registration is based on maximization of MI (A,B) (equation 1). The entropies (marginal and joint) are from [9],

$$p_{A,B}(a,b) = h(a,b) \Big/ \sum_{a,b} h(a,b) \tag{2}$$

$$H(B) = \sum_{b} -p_B(b) \log p_B(b) \tag{3}$$

$$H(A,B) = \sum_{a,b} -p_{A,B}(a,b) \log p_{A,B}(a,b) \tag{4}$$

Where $p_A(a)$ and $p_B(b)$ are the marginal probability mass functions and $p_{A,B}(a,b)$ is the joint probability mass function. These probability mass functions can be obtained from,

$$p_{A,B}(a,b) = h(a,b) \Big/ \sum_{a,b} h(a,b) \tag{5}$$

$$p_A(a) = \sum_{b} p_{A,B}(a,b) \tag{6}$$

$$p_B(b) = \sum_{a} p_{A,B}(a,b) \tag{7}$$

where h is a joint histogram (JH) of the two images involved. It is a 2D matrix with the intensity values of one image along one axis and the intensity values of the other image along the other axis. Thus, it can be seen from equations (1) to (7) that the joint histogram is the only requirement for MI computation between any two images. Here, we have employed the normalized MI implementation proposed in (Studholme et al. 1999). This reduces the sensitivity of MI towards changes in image overlap.

$$MI(A,B) = \big(H(A) + H(B)\big) \big/ H(A,B) \tag{8}$$

A mutual information based registration includes a careful selection of a joint histogram technique and an optimizer to find the registration parameters. For optimizing the registration function, input image might be transformed several times over the reference image grid. For many cases, the transformed input image might not coincide with the target reference image grid. Therefore, an exact joint histogram may not be obtained and some approximation becomes inevitable. For joint histogram estimation, one step and two step histogram techniques have been utilized in past (Chen et al. 2003). In general, the interpolation step of intensity values has been held responsible for introducing interpolation induced artefacts (Tsao, 2003), (Inglada et al. 2007) in MI function which makes the function optimization a tedious task. For the presented work, one step joint histogram technique namely generalized partial volume estimation (GPVE) (Chen et al. 2003) is utilized. A detailed evaluation of GPVE using different order B-spline kernels to estimate the joint histogram for high resolution SAR optical image chip matching can be found in (Suri et al. 2008). For selecting an optimizer, (Pluim et al. 2003) presents a survey of optimization techniques utilized in MI based registration. In this work, we have utilized the first order Simultaneous Perturbation Stochastic Approximation (SPSA) optimization scheme [Spall, 1999].

2.3 Different Sensor Geometries

To demonstrate the influence of different sensor geometries on intensity based registration we performed our analysis with high resolution imagery acquired over suburban area west of Munich, Germany. The images can be visualized in Figure 1 (a, b), the imaged scene has urban settlement situated very next to vast agricultural fields providing an opportunity to analyze the similarity metric performance for the two land covers, both combined and independent. For experimentation the following two scenarios have been considered:

For case 1, we select pixels only from the plain fields (roughly demarcated with rectangle in Figure 1) in both the images for computing the registration parameters (Size: 953 × 1096 pixels). For the plain field pixels the side-looking SAR sensor and the downward looking optical sensor are not expected to have much of their geometric influence, so favorable registration results as in the previous case are expected.

For case 2, we select the entire image scene for registration parameter computation and hence analyze the influence of the sub urban establishments on similarity metric performance (Size: 1001 × 2001 pixels). The urban establishments cause great changes in SAR image radiometry due to its sideways looking geometry.

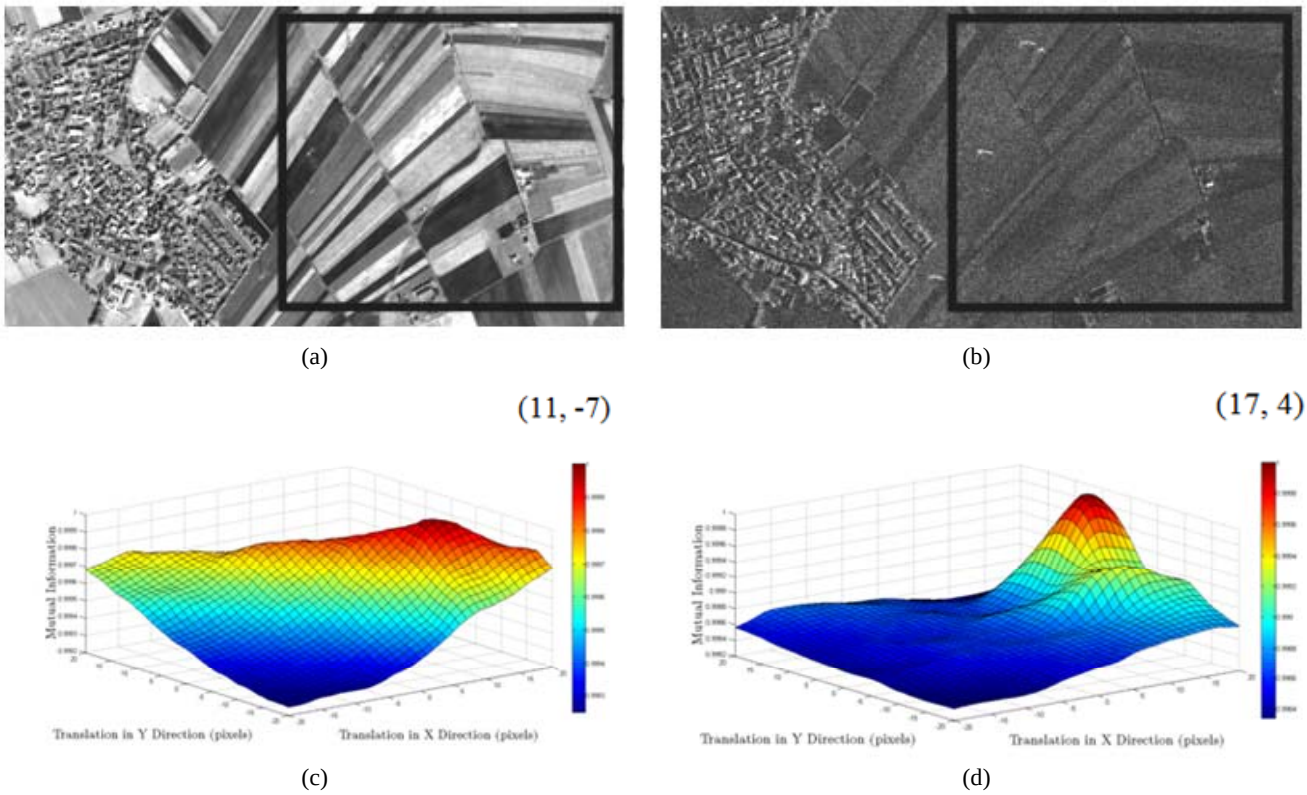

Figure 1. (a) The IKONOS and (b) TerraSAR-X imagery for dataset 2. (c) Plain field pixels lead to a registration peak of (11, -7) for MI. (d) Introduction of urban area pixels shifted the registration peaks for MI to (17, 4).

We move the input image (IKONOS) over the reference image (TerraSAR-X) in the range (Suri et al. 2010) pixels in both x and y direction, both the similarity metric functions have been recorded at integral pixel movements. For this experiment, joint histogram of bin size 64 has been estimated using the GPVE technique (Cubic B-spline kernel). The search spaces generated by both the metrics for the two cases are provided in Figure 1. The Figure 1c represents the generated search spaces for MI while utilizing pixels belonging only to the land cover class fields. Figure 1d represents the generated search spaces while utilizing the complete image region including the suburban areas.

Tests conducted with a bin size 64 only taking pixels from the plain fields, returned the registration peak at (11, -7) for MI (Figure 1c). On the other hand, the surfaces generated by utilizing all the pixels in both the images obtain a peak at (17, 4) (Figure 1d). A visual analysis using an overlay tool clearly indicates the present misalignment within the imagery after using the obtained registration parameters from case 2. Although the land cover fields constitute more than 53% of the total image area, still the introduction of the urban area pixels have derailed the registration process which is evident in the form of false registration peaks observed. This shift in the peaks can be attributed to high entropy content normally present with in urban areas which is also evident from the sharper false registration peaks obtained by both the similarity metrics in case 2.

This shift in the registration peaks of both the metrics can directly be related to the introduction of region greatly influenced by different sensor geometries. Theoretically, registration between two images is achieved by maximizing the similarity metric between two images. But due to the influence of different sensor geometries especially in urban, semi urban areas the peak obtained simply by the maximization process might not yield desirable results. The double bounce, triple bounce effect prominently observed in the SAR imagery at 1m resolution make the radiometric information produced by two sensors incompatible in urban areas and might lead to failure of intensity based techniques to detect correct registration parameters.

Normally, for practical applications land cover classes are hardly as segregated as available in the analyzed dataset. However, the presented scene is still a good selection to show the possible influence of different sensor geometries on an intensity based registration performance. This problem of mixed classes asks for a segmentation step before using intensity based techniques for registration parameter estimation. The segmentation should be targeted to incorporate only those pixels in the registration process which are not influenced by different sensor geometries (like the plain field pixels in the dataset). However, the idea of introducing a segmentation step before performing an intensity based registration has the following concerns to be addressed:

1. Supervised or unsupervised, ideally unsupervised would be preferred to avoid any kind of manual intervention in the registration process
2. The accuracy and the speed of the segmentation, it needs to be established that how much accuracy in segmentation is actually needed for robust performances.

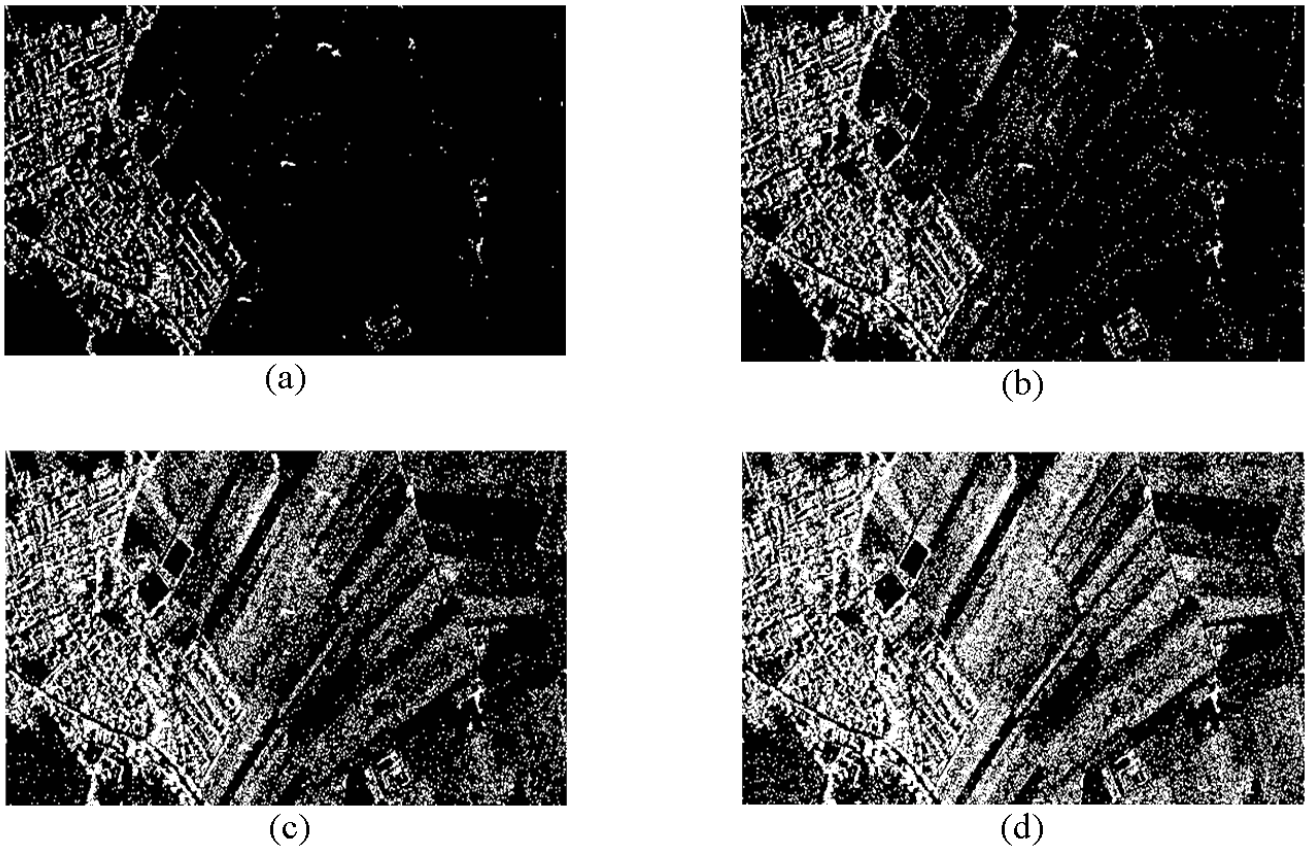

Figure 2. Pixels with value 1 were left out (in SAR image) of the registration process after introducing high thresholds of 5% (a) 10% (b) 20% (c) and 30% (d) at image compressed to one-forth of its original resolution

3. Segmentation required only in one image or both the images involved in the registration process

Considering the scenario, we propose here a method to successfully adapt intensity-based techniques for heterogeneous land cover scenes. The proposed method is unsupervised, very fast and easy to implement and requires segmentation in only one of the images being registered. The idea of the proposed solution lies in the histogram of a SAR image acquired over urban/semi-urban areas. Normally, the pixels produced by the double/triple bounce phenomenon result into a very strong backscatter to the radar sensor and thus these pixels always would be situated near the higher end of a SAR image histogram. Here it has to be kept in mind that certain other pixels, not generated by the SAR geometry - due to constructive interference of the radar waves - can also produce high intensity value (strong backscatter). However, it still might be possible to bin out most of the pixels explicitly generated due to the SAR sensor geometry using histogram thresholds. As already mentioned certain pixels (even in plain fields) as a result of constructive interference might also be binned out of the registration process. But as long as the numbers of such false pixels being binned out represent minority of the total pixel population, the registration peaks obtained by the similarity metrics are not expected to change. The number of such pixels can definitely be reduced by some kind of speckle filtering but intensity based registration of SAR and optical imagery does not require any necessary smoothing step so we refrain to perform the same in the presented approach.

To perform the necessary segmentation step we again revert to image compression, the advantages of performing the segmentation task in a coarser resolution SAR image are two folds:

1. Computational speedup: It is clear that the time complexity of the segmentation step is directly dependent upon the size of the image so image compression can be used to a good effect.
2. Image Smoothing: The utilized averaging block filter also introduces some kind of smoothing in the image so this in turn might help only binning out those pixels which are a result of sideways looking SAR sensor geometry

The proposed segmentation performed here can be visualized in Figure 2. First the SAR image (Figure 1b) is down-sampled to one-forth of its original resolution. The histogram of the obtained down-sampled image is now used to generate thresholds for binning out possible pixels generated by the SAR sensor geometry in the original resolution image. To realize the goal of the segmentation process thresholds are made from the higher end of the image histogram.

The result of this segmentation scheme has been represented as binary masks (value of 1 means the pixel is not included in the registration process) depicted in Figure 2 (a, b, c, d) represent the results of introducing thresholds of 5, 10, 20 and 30% on the down-sampled image (one-fourth of the original resolution).

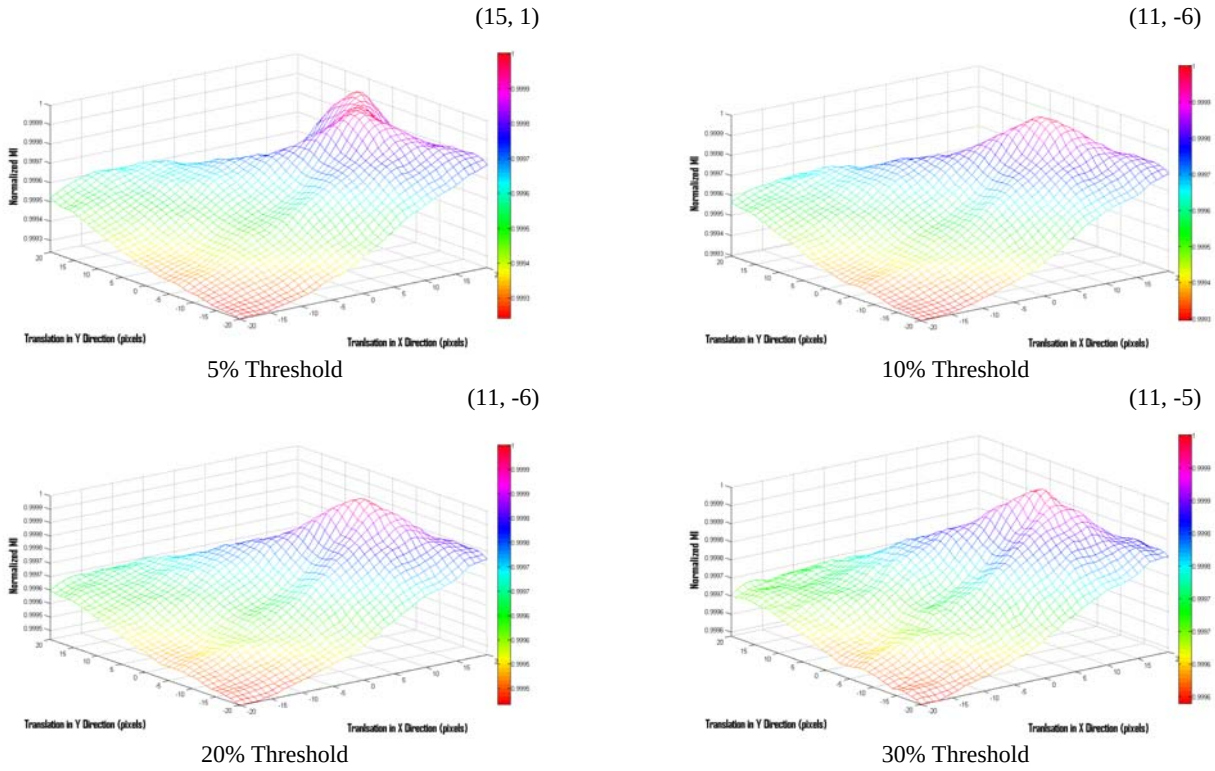

Figure 3. Registration surfaces generated by MI between segmented SAR (using masks from Figure 2) and the original optical image (shift value in brackets)

It can be clearly observed that as the threshold limit is relaxed more and more pixels from the plain fields start coming into the undesired pixel category and this might have an adverse influence on similarity metric performance.

To analyze the influence of the performed segmentation we repeat the same experiment as done earlier. The idea here is to register the segmented SAR image with the corresponding optical image. In this scenario all the pixels from optical imagery would contribute to the similarity metric statistics but from the SAR imagery only those pixels which are within the threshold limits (assigned the value 0 in the masks of Figure 2) would participate in the registration process. To analyze the threshold value influence on the final registration results and similarity metric performances we repeat the same experiment with different threshold levels (Figure 2). The similarity metric surfaces generated in the search space of (Suri et al. 2010) pixels for the segmented SAR images and the original optical image have been provided in Figure 3 for visualization and analysis.

The influence of the introduced segmentation step prior to intensity based registration is evident on the registration search spaces generated in Figure 2. Segmentation of the SAR image using the mask depicted in Figure 3a (5% threshold) influenced the registration peaks observed in Figure 1d significantly. The registration peaks obtained by MI (17, 4) in Figure 1d was shifted to (15, 1). Further segmentation of the SAR image that is using threshold in the order of 10, 20 and 30% percent yielded almost the same registration peaks as were reported by the similarity metrics using only the pixels from plain fields (Figure 1c). The MI peaks obtained for the segmented SAR and the optical imagery deviate only about 1 m from the peaks obtained earlier using only the plain field pixels, which in this case are assumed to be the true on ground registration parameters.

The segmentation strategy introduced in this section has yielded encouraging registration performances from both the similarity metrics. It can be observed that very loose threshold of 5% could remove only some of the pixels influenced by the SAR sensor geometry and thus did not produce expected registration results. On further tightening the thresholds to higher levels, most of the pixels influenced by SAR sensor geometry (mostly in the urban settlement) were removed and expected registration parameters were successfully retrieved.

3. SENSOR ORIENTATION

Considering high precision position determination of satellite systems (increasingly sub-meter range position accuracies become state-of-the art) as well as stable interior orientation of camera systems the improvement of satellite attitude / sensor alignment using GCPs is one of the major tasks. Especially thermal effects caused by the sun exposure time during satellite orbit revolution influences the relative alignment between the body and the sensor coordinate frames and leads to pointing errors. A thermal stable connection between the camera system and the attitude measurement system like star trackers as well as a compact assembly with close distances between the devices is often hard to establish, which results in a thermal sensitive behaviour. Therefore by iterative least squares adjustment improved alignment angles can be estimated and introduced in the extended physical sensor model (Müller et al. 2005). The improved sensor model is finally applied to orthorectify the optical data by object point reconstruction using interpolated

terrain height values from the DEM and by transformation of planar object points to a map projection including appropriate pixel value resampling within a regular grid.

3.1 RPC correction

Exterior and interior orientation can be implicitly encoded in form of rational polynomial functions (RPF) using third order polynomials for nominator and denominator (80 coefficients). This Universal Sensor Model (USM) provides the transformation of object space coordinates to image space coordinates, which is available in standard format for a lot of remote sensing satellite systems. Each of the RPF for row and column is given via a ratio of 2 polynomials of third order in normalized λ, φ, and h with 20 coefficients.

$$r = rpf_r(\lambda, \varphi, h)$$
$$c = rpf_c(\lambda, \varphi, h) \quad (9)$$

where *r/c* are row and column coordinates of the image and λ, φ, and h are longitude, latitude and ellipsoidal height in geographic coordinates of WGS84 datum.

In order to improve the geometric accuracy of the original RPC, these have to be corrected via ground control information. An affine transformation is estimated by least squares adjustment via the GCP derived from image matching between satellite scene and the reference scene. The corrected image coordinates are calculated based on this affine transformation and the RPF given by

$$row = a_0 + a_1 \cdot rpf_r + a_2 \cdot rpc_c$$
$$col = b_0 + b_1 \cdot rpf_r + b_2 \cdot rpf_c \quad (10)$$

where rpf_r and rpf_c are the originally provided rational polynomial functions [Lehner et al. 2005].

3.2 Blunder detection

Different levels of blunder detection are included in the process chain to determine a set of GCPs of high geometric quality. A method for blunder detection is integrated in the least squares adjustment, which eliminates iteratively step by step GCPs with a residual greater than a threshold starting with the bottom quality GCP. In this context a residual is defined as deviation of GCP coordinates from the re-calculated object point coordinates using the refined sensor model, which has been derived from the adjustment using all currently valid GCPs. In a first step the whole GCP set serves as input for the iterative parameter estimation. Successively the GCP with bottom quality and residuals greater than a threshold is removed from the GCP set. This iterative procedure is repeated until a GCP set remains, which is consistent to the sensor model. The procedure has to be iterative, because each GCP influences the result of the parameter estimation. As threshold for the GCP blunder detection two pixel sizes have to be found as sufficient for ALOS / PRISM and IKONOS images (other values like 1 pixel size threshold show no significant improvement of blunder detection). The drawback of this method is that systematic errors for the majority of the GCPs can lead to erroneous or shifted values of the estimated parameters. Another possibility is the fact that we might obtain a poor distribution of the GCPs concentrated in only one part of the scene and a model estimated from such a distribution might not be ideal and consistent for the entire coverage.

4. APPLICATION EXAMPLES

The method explained in the last section has been applied to several data sets (see also (Reinartz et al. 2009), (Suri et al. 2010). In the following one example and results where the TerraSAR-X data have been used in the described ways, are shown for an ALOS-PRISM data set. These data sets have been chosen since the largest overlapping of the scenes and the best fitting independent ground control has been available.

4.1 Manual GCP measurements

In this section, the potential of manual GCP measurement is examined. Therefore, a test area near Marseille, France, was chosen. An ALOS PRISM nadir scene recorded on March 12, 2007 with 2.5 m GSD and a TerraSAR-X Stripmap scene recorded on April 20, 2009 with a GSD of 1.25 m were used for the test. Additionally, 25 GCPs measured with GPS were available.

For the test, 10 tie points were measured in both the TerraSAR-X and the PRISM scene. These points were used as GCPs to correct the orientation of the PRISM scene as described in section 3. The PRISM scene was then orthorectified using the corrected orientation. Another orthoimage was generated by correcting the orientation using 8 of the GPS points as GCPs. Figure 4 shows an overlay of these orthoimages.

The gray color indicates a very high consistency of both orthorectified images. This holds also true in mountainous areas. In order to assess the geometric accuracy of the orthorectified scene using GCP information extracted from the TerraSAR-X imagery, the GPS points were manually measured in the orthoimage. Table 1 shows the results.

Figure 4. Overlay of orthoimages. The blue and green channels show the orthoimage created with the GPS points, the red channel the one created using the TerraSAR-X points as GCPs. There are only very small visually detectable colour edges found.

	x	y
Bias [m]	1.7	3.4
Standard deviation [m]	2.6	3.0
RMSE [m]	3.1	4.5

Table 1. Statistics at 25 check points (GPS measurements)

4.2 GCP extraction by image matching

To evaluate the performance of the MI based approach presented in section 2.2, an automated processing chain was implemented and tested using the same dataset utilized for the manual GCP measurements in section 5.1.

This processing chain starts by generating an equidistant grid of points in the original PRISM image. To facilitate MI matching of these points with the reference TerraSAR-X scene, the PRISM image is orthorectified using the uncorrected attitude information (Mean shift compared to the reference GPS points: 24.7 m in x; 84.44 m in y). Next, the found matches are used to estimate more accurate attitude angles as described in section 3. Moreover, during this step wrong and inaccurate matches are eliminated. Finally, the improved sensor model is used to orthorectify the PRISM scene.

For the MI statistic computation a window with a size of 400x400 pixels is employed, using a Sextic B-Spline Kernel for joint histogram estimation (Suri et al. 2008). 122 grid points were generated automatically, out of which 109 remained after MI matching (selected on the basis of individual match consistency). The corrections obtained by MI can be seen in Figure 5. During the sensor model improvement step another 38 points were discarded based on a threshold of 2.0 pixels, finally leading to 71 remaining matches with a RMSE of these points 0.73 pixel in x and 0.86 pixel in y relative to the computed model.

When compared to the 25 independent high precision GPS points a mean deviation of -2.8 m and -8.0 m in x and y respectively was obtained (Table 2). While the mean deviation has not yet achieved results as good as those obtained manually, the comparably low standard deviation (x: 2,6m; y: 2,0m) indicates a good matching consistency.

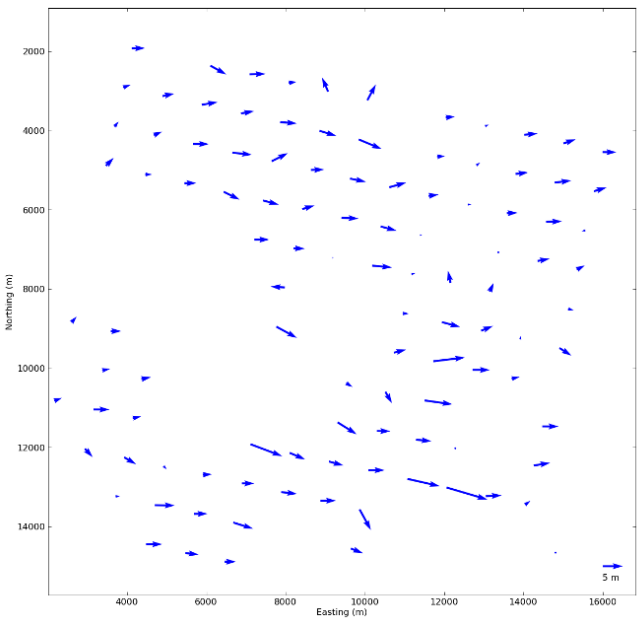

Figure 5. Shifts of matches computed by MI compared to their initial position (arrow lengths are scaled by a factor 100)

	x	y
Bias [m]	2.8	8.0
Standard deviation [m]	2.6	2.0
RMSE [m]	3.8	8.2

Table 2. Statistics at 25 check points (GPS measurements)

Further investigations have been performed and are published in IEEE Transactions on Geoscience and Remote Sensing (Special issue on TerraSAR-X) (Suri et al. 2009).

5. CONCLUSIONS

For combined utilization of data from diverse natured sensors automatic co-registration methods are a must as satellite images may have georeferencing differences of magnitude that might influence any analysis or decision making process. Considering the meticulous task of extracting and matching conjugate features in SAR and optical imagery (especially metric resolution imagery) a general feature based image registration technique for various scenarios might be difficult to develop and implement. On the other hand, the intensity based metrics for medium resolution images (5-15 m GSD) have shown enough potential of suitably being modified and extended for different registration scenarios.

In this paper we have investigated the performance of intensity based registration techniques for high and very high resolution imagery acquired by TerraSAR-X and ALOS/PRISM as well as IKONOS satellites. As was expected the different radiometric information contained in the two images due to different sensor geometry and radiometry did hamper the intensity based techniques but suitable solutions have been proposed for handling the same.

It has been shown that TerraSAR-X data can be used as an information source for absolute orientation improvement for high resolution optical satellite data. In the displayed example the manual measurement of conjugate points leads to an absolute geolocation accuracy of better than 5 m (equivalent to two pixels for ALOS-PRISM data), checked at totally independent GCP. While automatic matching techniques, using mutual information registration, show a high matching consistency (approx. 1 pixel), the absolute geolocation error is in the order of 8 m. The reason for this discrepancy has to be studied in more detail and checked with other data sets. The intended study will include a detailed evaluation of MI SAR optical image matching capability by analyzing various window sizes, joint histogramming and thresholding techniques for different land cover classes.

The absolute geolocation accuracy of TerraSAR-X EEC data can be only as good as the DEM used for the production, since the measured range values depend on the accuracy of the underlying DEM. This could possibly lead to the above mentioned discrepancies. In further investigations, areas will be chosen where the absolute geometric accuracy of the TerraSAR-X EEC data is known to be very high and several techniques for automatic extraction of tie points using mutual information will be used.

REFERENCES

Ager T., Bresnahan P., 2009, “Geometric Precision in Space Radar Imaging: Results from TerraSAR-X”, NGA CCAP report.

Chen H. and Varshney P. K., 2003, "Mutual information-based CT-MR brain image registration using generalized partial volume joint histogram estimation," IEEE Trans. on Medical Imaging, vol. 22, pp. 1111-1119

Chen H., Varshney P. K. and Arora M. K., 2003, “Performance of mutual information similarity measure for registration of multitemporal remote sensing images”, IEEE Trans. on Geoscience and Remote Sensing, vol. 41, no 11, pp. 2445-2454

Collignon A., Maes F., Delaere D., Vandermeulen D., Suetens P. and Marchal G., 1995, "Automated multimodality image registration based on information theory", Information Processing in Medical Imaging (Y. Bizais, C. Barillot and R. Di Paola, eds.), Kluwer Academic Publishers, Dordrecht, pp. 263-274

Inglada J., Muron V., Pichard D. and Feuvrier T., 2007, “Analysis of artifacts in subpixel remote sensing image registration”, IEEE Trans. on Geoscience and Remote Sensing, vol. 45, no. 1, pp. 254-264

Jacobsen K., 2006, “Pros and Cons of the Orientation of Very High Resolution Optical Space Images”, IntArchPhRS. Band XXXVI 1/ WG I/5. Paris, 7p.

Lehner M., Müller R., Reinartz P., June 2005, “DSM and Orthoimages from QuickBird and IKONOS Data Using Rational Polynomial Functions”, Proceedings of ISPRS Hannover Workshop, High Resolution Earth Imaging for Geospatial Information, Commission I, WG 5, 6p, on CDROM

Müller R., Krauß T., Lehner M., and Reinartz P., May 2007, Automatic Production Of A European Orthoimage Coverage Within The GMES Land Fast Track Service Using Spot 4/5 And IRS-P6 Liss III Data, ISPRS Conference Proceedings, Volume XXXXVI, ISPRS Workshop Hannover, Germany, 6 p.

Müller R., Lehner M., Reinartz P., Schroeder M., June 2005, „Evaluation of Spaceborne and Airborne Line Scanner Images using a generic Ortho Image Processor”, Proceedings of ISPRS Hannover Workshop, High Resolution Earth Imaging for Geospatial Information, Commission I, WG 5, 6p, on CDROM.

Pluim J., Maintz J., and Viergever M., 2003, “Mutual Information Based Registration of Medical Images: A Survey”, IEEE Trans. on Medical Imaging, vol. 22, no. 8, pp. 986-1004

Reinartz P., Müller R., Lehner M., Schroeder M., 2006, “Accuracy Analysis for DSM and orthoimages Derived from SPOT HRS Stereo Data using direct georeferencing”, ISPRS Journal of Photogrammetry and Remote Sensing, Vol. 60/3, pp. 160-169.

Reinartz P., Müller R., Suri S., Schneider M., Bamler R., 2009, Using Geometric Accuracy Of TerrasSAR-X Data for Improvement of Direct Sensor Orientation and Ortho-Rectification of Optical Satellite Data, IGARSS, Cape Town, South Africa, 5p., on CDROM

Schubert A., Jehle M., Small D., Meier E., Nov. 2008 “Geometric Validation of TerraSAR-X High-resolution Products”, Proc. of TerraSAR-X Science Team Meeting, Oberpfaffenhofen, Germany, 6p.

Spall J. C., 1999, “Multivariate stochastic approximation using a simultaneous perturbation gradient approximation”, IEEE Transactions On Automatic Control, vol. 37, 332-341

Studholme C., Hill D. L. G. and Hawkes D. J., 1999, “An overlap invariant entropy measure of 3D medical image alignment”, Pattern Recognition, vol. 32, no. 1, 71–86

Suri S., Reinartz P., 2009, “On the Possibility of Intensity Based Registration for Metric Resolution SAR and Optical Imagery”, 12th AGILE International Conference on Geographic Information Science, Leibniz Universität Hannover, Germany, on CDROM

Suri S., Reinartz P., 2010, “Mutual Information based registration of TerraSAR-X and IKONOS imagery in urban area”, accepted in IEEE Transactions on Geoscience and Remote Sensing (Special Issue: TerraSAR-X), 48 (2), 939-949

Suri S., Reinartz P., June 2008, “Application of Generalized Partial Volume Estimation for Mutual Information based Registration of High Resolution SAR and Optical Imagery”, Proceedings of Fusion Conference 2008, Cologne, Germany, 8 p.

Tsao J., 2003, “Interpolation artifacts in multimodality image registration based on maximization of mutual information”, IEEE Trans. On Medical Imaging, vol. 22, no. 7, pp. 854-864

Viola P. A., 1995, “Alignment by maximization of Mutual Information”, PhD Thesis, Artificial Intelligence Laboratory, Massachusetts Institute of Technology, http://research.microsoft.com/~viola/Pubs/MIT/PHD-thesis.pdf, 156p. (Accessed, March 22, 2009).